Article

Adsorption Behaviors of Chlorosilanes, HCl, and H$_2$ on the Si(100) Surface: A First-Principles Study

Yajun Wang, Zhifeng Nie,* Qijun Guo, Yumin Song, and Li Liu

Read Online

ACCESS | Metrics & More | Article Recommendations

ABSTRACT: The hydrochlorination process is a necessary technological step for the production of polycrystalline silicon using the Siemens method. In this work, the adsorption behaviors of silicon tetrachloride (SiCl$_4$), silicon dichloride (SiCl$_2$), dichlorosilane (SiH$_2$Cl$_2$), trichlorosilane (SiHCl$_3$), HCl, and H$_2$ on the Si(100) surface were investigated by first-principles calculations. The different adsorption sites and adsorption orientations were taken into account. The adsorption energy, charge transfer, and electronic properties of different adsorption systems were systematically analyzed. The results show that all of the molecules undergo dissociative chemisorption at appropriate adsorption sites, and SiHCl$_3$ has the largest adsorption strength. The analysis of charge transfer indicates that all of the adsorbed molecules behave as electron acceptors. Furthermore, strong interactions can be found between gas molecules and the Si(100) surface as proved by the analysis of electronic properties. In addition, SiCl$_2$ can be formed by the dissociation of SiCl$_4$, SiH$_2$Cl$_2$, and SiHCl$_3$. The transformation process from SiCl$_4$ to SiCl$_2$ is exothermic without any energy barrier. While SiH$_2$Cl$_2$ and SiHCl$_3$ can be spontaneously dissociated into SiHCl$_2$, SiHCl$_2$ should overcome about 110 kJ/mol energy barrier to form SiCl$_2$. Our works can provide theoretical guidance for hydrochlorination of SiCl$_4$ in the experimental method.
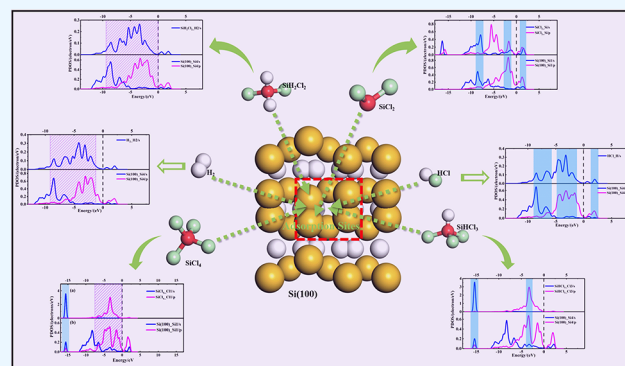
1. INTRODUCTION

Polycrystalline silicon has been regarded as the critical raw material for solar cell manufacturing,[1,2] and the Siemens process is widely used to produce polycrystalline silicon.[3] However, the entire process produces large amounts of silicon tetrachloride (SiCl$_4$) and HCl as byproducts.[4,5] By employing hydrogenation technology, this excess SiCl$_4$ can be converted back into useful trichlorosilane (SiHCl$_3$), which is the starting material for chemical vapor deposition of polycrystalline silicon.[6,7] In general, there are two hydrogenation routes, namely, thermal hydrogenation[8] and hydrochlorination.[9] The first route involves the hydrogenation of SiCl$_4$ at a high temperature (>1373 K).[8] The overall reaction is

$$SiCl_4(g) + H_2(g) \rightarrow SiHCl_3(g) + HCl(g) \qquad (1)$$
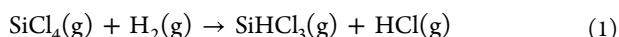
The second one is known as hydrochlorination,[10,11] which has a lower energy consumption and higher conversion in comparison with thermal hydrogenation. The reacting system is as follows

$$3SiCl_4(g) + Si(s) + H_2(g) \rightarrow 4SiHCl_3(g) + HCl(g) \qquad (2)$$
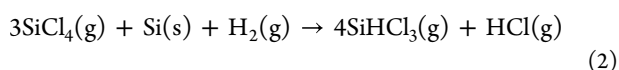
However, the hydrochlorination of SiCl$_4$ is relatively complex,[12,13] and there are some intermediate products generated during the formation of SiHCl$_3$, such as SiCl$_2$,[14]

SiH$_2$Cl$_2$,[15] and so on. There is still no consensus about the complex reactions which can occur, especially concerning the gas−silicon surface interactions. Currently, the first-principles calculations can effectively reveal the microcosmic interactions of the gas−silicon surface.

The Si(100) surface is proved to be very stable because of the low surface energy, and it undergoes reconstruction after full relaxation, i.e., the undercoordinated surface Si atom pair usually results in the formation of dimers.[16,17] Therefore, the interactions between the active silicon surface and gas molecules have received extensive investigations. For instance, Hall et al.[18] used the density functional theory (DFT) method to study the adsorption behaviors of chlorosilanes (SiH$_2$Cl$_2$, SiHCl$_3$, and SiCl$_4$) on the Si(100) surface and found that the scission of SiH$_2$Cl$_2$ and SiHCl$_3$ is more inclined to pass through the Si−Cl bond instead of the Si−H bond. Ng et al.[19] employed the DFT computation to investigate the micro-
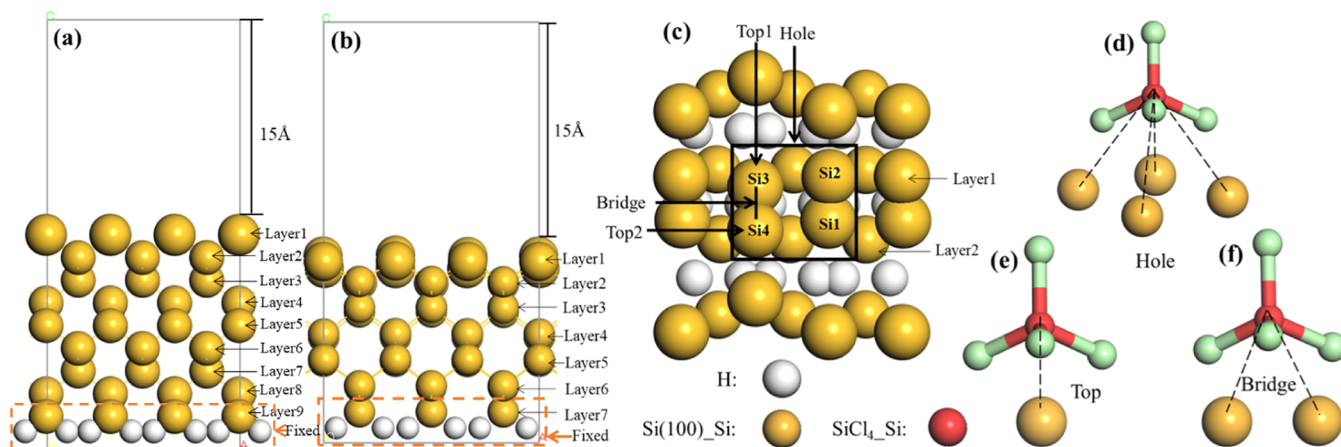
Figure 1. (a) Nine atomic layers of the Si(100) structure and (b) side view and (c) top view of seven atomic layers of the Si(100) structure, and different adsorption styles for the SiCl$_4$ molecule: (d) hole site, (e) top site, and (f) bridge site.

cosmic mechanism for disilane (Si$_2$H$_6$) adsorption on Si(100). They found that Si$_2$H$_6$ is dissociative adsorbed on the Si(100) surface, and the Si−H bonds are more prone to rupture compared with Si−Si bonds. Besides, some interesting phenomena can be observed after single-molecule adsorption on Si(100). For example, the SiCl$_2$, SiCl$_3$, and SiCl$_4$ clusters can be formed after the Si atom is adsorbed on the chlorinated Si(100) surface.[20] When the Cl atom is adsorbed on the Si(100) surface under ultrahigh vacuum conditions, the dissociated Cl$_2$ and the active Cl radicals can lead to the formation of SiCl$_4$.[21] Additionally, in contrast with the dissociative adsorption suggested by some available kinetic models, Anzai et al.[22] indicated that SiCl$_2$ undergoes molecular adsorption at the Si(100) surface. However, the systematic investigations on the adsorption and reaction mechanism of byproducts generated by the Siemens process (including chlorosilanes, HCl, and H$_2$) on the Si(100) surface are still lacking, which is difficult to be studied by the traditional experimental method.

Therefore, the first-principles calculations were adopted to simulate the adsorption behaviors of chlorosilanes (SiCl$_4$, SiCl$_2$, SiH$_2$Cl$_2$, and SiHCl$_3$), H$_2$, and HCl on the Si(100) surface in this work, which aims to reveal the gas−silicon surface interactions in the hydrochlorination process of SiCl$_4$. The adsorption energy, charge transfer, and electronic properties, including total charge density (TCD), charge density difference (CDD), and density of states (DOS) of the gas−silicon surface, were also revealed. The results of this study help to provide a theoretical basis for exploring the reaction mechanism and experimental work of the hydrochlorination of SiCl$_4$.

2. CALCULATION METHODS AND MODELS

2.1. Calculation Method. In this work, the Dmol^3 package[23,24] with the dual numerical plus polarization (DNP) basis set was used to perform all of the DFT calculations.[25] To treat the electron change and correlation interactions,[26] the Perdew−Burke−Ernzerhof (PBE)[27−30] form of the generalized gradient approximation (GGA) functional[31,32] was selected. Specifically, the Brillouin zone integrations were performed using a Monkhorst−Pack grid of 6 × 6 × 1 k points, and all calculations were nonspin polarized.[33] We chose the 4.6 Å cutoff radius for geometry optimization, where a smearing value of 0.005 Ha was

employed for rapid convergence. Effective core potential (ECP) of the Hartree−Fock potential is used to treat inner electrons.[34] When the force of relaxed atoms is lower than 5 × 10^{-5} Ha, SCF tolerance is lower than 5 × 10^{-6} Ha, the force change between two steps is smaller than 0.02 Ha/Å, and the atomic structures tend to be stable. To avoid the interaction of each layer during the calculations, a vacuum layer thickness of 15 Å was added to the top of the Si(100) surface.[35] The adsorption energy (E_{ads}) is calculated as follows

$$E_{ads} = E_{gas/Si(100)} - E_{gas} - E_{Si(100)} \tag{3}$$

where $E_{gas/Si(100)}$ is the total energy of Si(100) with gas adsorption and E_{gas} and $E_{Si(100)}$ are the total energies of the isolated gas molecule and Si(100) surface, respectively.

The charge density difference ($\Delta\rho$) is calculated using the following expression

$$\Delta\rho = \rho_{gas/Si(100)} - \rho_{gas} - \rho_{Si(100)} \tag{4}$$

where $\rho_{gas/Si(100)}$, ρ_{gas}, and $\rho_{Si(100)}$ are the charge density of gas adsorbed on the Si(100) surface, free gas molecule, and Si(100) surface, respectively.

2.2. Surface Model. Silicon (Si) has a diamond-like and tetrahedral structure, and the optimized lattice parameter (5.470 Å) and bulk modulus (91.1 GPa) in this work are consistent with the experimental result (5.500 Å[36] and 97.8 GPa[37]). The adsorption energies of SiCl$_4$ on seven and nine[38−40] atomic layers (Figure 1a,b) at the top1 site were calculated. Both cases belong to dissociative adsorption (SiCl$_3$* + Cl*), and the slab with seven atomic layers is large enough. Thus, to improve the calculated efficiency, seven atomic layers of Si(100) were selected in this work. Si(100) is modeled with $p(3 \times 3)$ supercells with seven atomic layers, and the surface energy is calculated to be 153 mJ/m^2, which is also close to the theoretical values[41] of 100−200 mJ/m^2. Our calculation results are in good agreement with the experimental and theoretical values, which verifies the accuracy of this calculation. The bottom layer was passivated with two hydrogen atoms per silicon atom, as shown in Figure 1a. During the calculation process, the bottom two layer atoms are fixed,[29,42] and the other layer atoms and adsorbed molecules are relaxed. Figure 1 shows the Si(100) surface structure, which contains the three dimers, and the middle dimer is selected as the adsorption site. To determine the most stable structure of gas molecules on Si(100), four possible adsorption

sites are considered, including top1 (top of Si3), top2 (top of Si4), bridge (bridge site of the Si3−Si4 bond), and hole (central site of the middle dimer) sites, as shown in Figure 1b, and the four Si atoms in the first layer are marked with "Si1", "Si2", "Si3", and "Si4", respectively. Taking the SiCl$_4$ molecule as an example, the adsorption styles of gas molecules are plotted in Figure 1d−f.

3. RESULTS AND DISCUSSION

3.1. Stability and Geometric Structures. First, we calculate the adsorption energy of gas molecules on the Si(100) surface at different adsorption sites, as listed in Table 1. One can see that SiCl$_4$, SiCl$_2$, SiH$_2$Cl$_2$, SiHCl$_3$, HCl, and H$_2$

Table 1. Adsorption Energies and Corresponding Adsorption Products on Different Adsorption Sites of the Si(100) Surface[a]

molecule	adsorption site	reaction products	E_{ads} (eV)
SiCl$_4$	top1	SiCl$_3$* + Cl*	−1.57
	top2	SiCl$_3$* + Cl*	−1.73
	bridge	SiCl$_2$* + 2Cl*	−2.46
	hole	SiCl* + 3Cl*	−1.99
SiCl$_2$	top1	SiCl$_2$*	−1.88
	top2	SiCl$_2$*	−2.18
	bridge	SiCl$_2$*	−2.06
	hole	SiCl* + Cl*	−2.17
SiH$_2$Cl$_2$	top1	SiH$_2$Cl* + Cl*	−1.47
	top2	SiH$_2$Cl$_2$*	−0.18
	bridge	SiH$_2$Cl$_2$*	−0.19
	hole	SiHCl$_2$* + H*	−1.86
SiHCl$_3$	top1	SiHCl$_2$* + Cl*	−1.96
	top2	SiHCl$_2$* + Cl*	−1.91
	bridge	SiHCl$_2$* + Cl*	−1.82
	hole	SiHCl* + 2Cl*	−2.63
HCl	top1	H* + Cl*	−2.60
	top2	HCl*	−0.10
	bridge	HCl*	−0.11
	hole	H* + Cl*	−2.59
H$_2$	top1	H$_2$*	−0.08
	top2	H$_2$*	−0.09
	bridge	2H*	−1.96
	hole	H$_2$*	−0.09

[a]Here, * denotes a surface site.

molecules are preferentially adsorbed at the bridge, top2, hole, hole, top1, and bridge sites with the E_{ads} of −2.46, −2.18, −1.86, −2.63, −2.60, and −1.96 eV, respectively. Moreover, the adsorption strength of SiHCl$_3$ is larger than those of the other gas molecules (SiCl$_4$, SiCl$_2$, SiH$_2$Cl$_2$, HCl, and H$_2$) due to the higher adsorption energy.

Figure 2 gives the most stable configurations of SiCl$_4$, SiCl$_2$, SiH$_2$Cl$_2$, SiHCl$_3$, HCl, and H$_2$ adsorbed on the Si(100) surface. We can find that most of the molecules are dissociative adsorption on Si(100) except for the SiCl$_2$ molecule, and all of the gas molecules strongly interact with the Si(100) surface by a chemical bond. This outcome indicates that those adsorption processes belong to chemisorption. The SiCl$_4$ molecule can be spontaneously dissociated into SiCl$_2$ and two Cl atoms as plotted in Figure 2a1,b1, and the bond length of Si−Cl1 and Si−Cl4 is stretched from 2.043 Å (experimental result is 2.090 Å[43]) to 5.177 and 3.906 Å, respectively. For the SiCl$_2$ molecule, it is vertically adsorbed on the surface, and the Si

atom of SiCl$_2$ bonds with two nearest-neighbor Si atoms of the Si(100) surface, which matches well with the results obtained by Anzai.[22] In addition, the SiH$_2$Cl$_2$ molecule spontaneously dissociates into SiHCl$_2$ and one H atom, while the SiHCl$_3$ molecule dissociates into SiHCl and two Cl atoms, as shown in Figure 2a3,a4. Also, the HCl and H$_2$ molecules are spontaneously dissociated into a single atom (H and Cl) after full relaxation, and the decomposed H and Cl atoms bond with Si atoms of Si(100).

The charge transfer (ΔQ) can be employed to evaluate the interaction strength between gas molecules and the Si(100) surface,[44,45] and it should be pointed out that the negative (positive) value means the gas molecule gains (loses) electrons. The charge transfer number for adsorption systems is correlated with different adsorption sites. Table 2 gives out the calculated ΔQ of the most stable adsorption systems based on the Hirshfeld charge. One can see that the electrons transferred from the Si(100) surface to SiCl$_4$, SiCl$_2$, SiH$_2$Cl$_2$, SiHCl$_3$, HCl, and H$_2$ molecules are 0.241, 0.061, 0.109, 0.288, 0.214, and 0.136 e, respectively. This outcome indicates that all of the gas molecules behave as electron acceptors, while the Si(100) surfaces act as electron donors. From Table 2, the SiHCl$_3$ gas molecule obtains the maximum electrons and thus exhibits the largest adsorption strength, which agrees well with the above results of E_{ads}.

3.2. Adsorption of Chlorosilane Molecules on the Si(100) Surface. To further understand the microcosmic interactions of the gas−silicon surface, the total charge density (TCD) and charge density difference (CDD) of the SiCl$_4$−Si(100) adsorption system were calculated and are shown in Figure 3. The strong overlapping of TCD can be found between SiCl$_4$ and the Si(100) surface (shown in Figure 3a), which indicates that the SiCl$_4$ molecule strongly interacts with the Si(100) surface. Moreover, from Figure 3b, there are large blue regions around SiCl$_4$, which indicates that a large number of electrons are transferred from the Si(100) surface to SiCl$_4$. Thus, the SiCl$_4$ molecule acts as an electron acceptor, which agrees well with the results of Hirshfeld charge analysis.

Figure 4 displays the total density of states (TDOS) of the SiCl$_4$−Si(100) adsorption system. As presented in Figure 4a,b, the TDOS curve shifts to the left as a whole after SiCl$_4$ adsorption, resulting in a decrease of total electron energy and making the electron more localized. After adsorption, the TDOS of SiCl$_4$ shifts to lower energy and the peaks become broader and lower, making the electron more delocalized. Moreover, the number of peaks is reduced after SiCl$_4$ adsorption, and the adsorbed SiCl$_4$ molecule saturates the Si atoms of the Si(100) surface, which indicates that the SiCl$_4$ molecule can be stably adsorbed on the Si(100) surface. As shown in Figure 4b,c, the orbital hybridizations between SiCl$_4$ and Si(100) mainly occur in the range of −12.50 to 0 eV (the green slash box area), and two resonance peaks can be observed at about −15.60 and 1.88 eV (the blue dashed outline), leading to the strong interaction between SiCl$_4$ and the Si(100) surface. Also, there are small peaks in the range of −17 to −15 eV (the red shaded area), and these peaks are contributed from SiCl$_4$.

The partial density of states (PDOS) of the SiCl$_4$−Si(100) adsorption system is plotted in Figure 5. In Figure 5a,b, there is a resonance peak at −15.6 eV (the blue shaded area), which illustrates that the dissociated Cl1 atom from SiCl$_4$ strongly interacts with the Si1 atom of the Si(100) surface. Meanwhile, it can be seen that there is an obvious electron orbital overlap
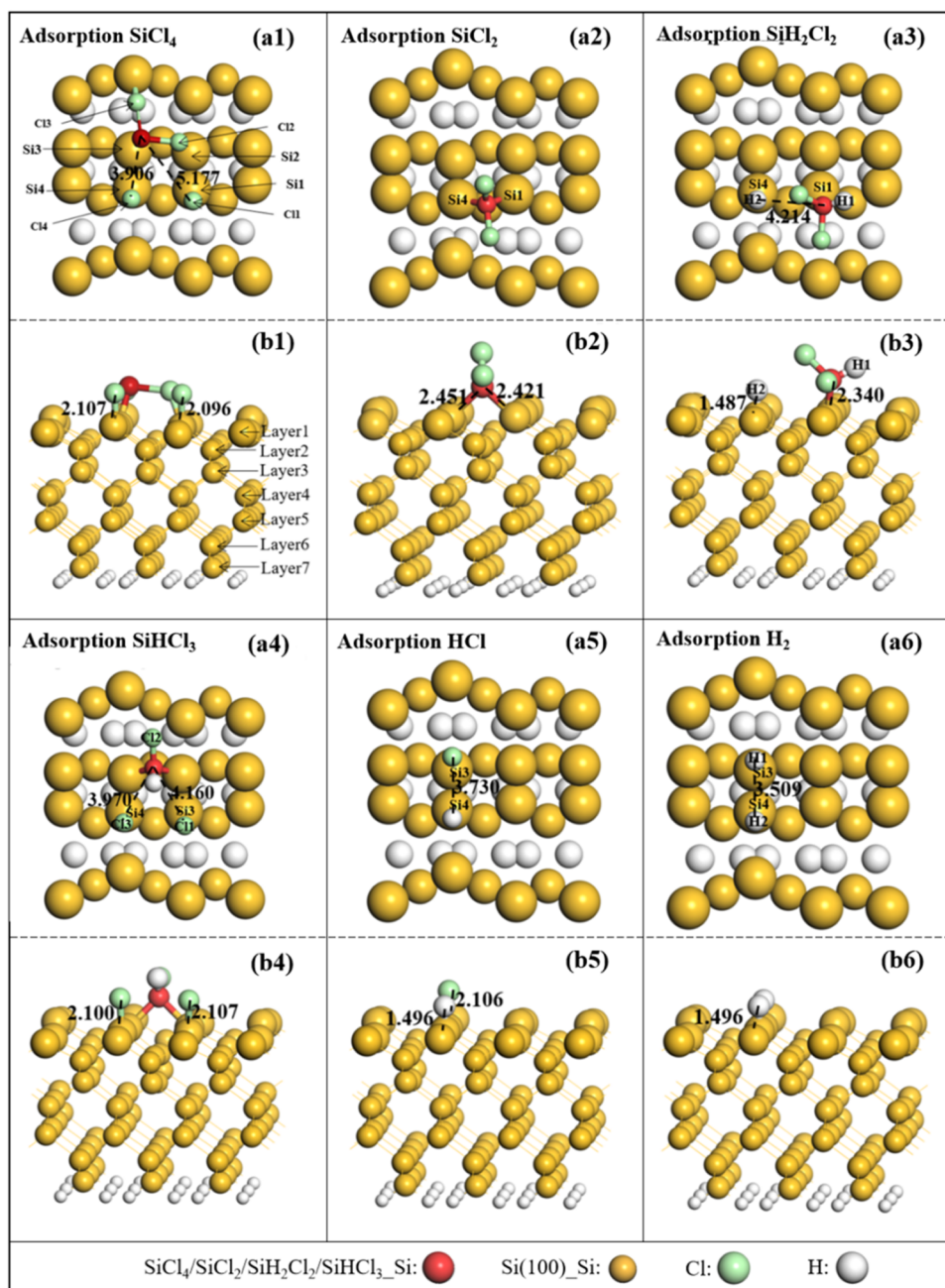
Figure 2. Top view (a1−a6) and side view (b1−b6) of the lowest-energy structures of different gas molecules absorbed on the Si(100) surface. The unit of bond length is Å.

Table 2. Charge Number (ΔQ, e) Transferred from the Si(100) Surface to Different Molecules for the Most Stable Adsorption Systems[a]

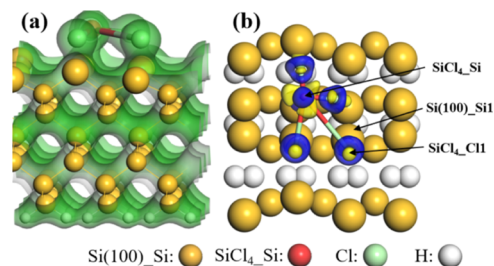| molecule	adsorption site	reaction products	ΔQ (e)
$SiCl_4$	bridge	$SiCl_2$* + 2Cl*	−2.46
$SiCl_2$	top2	$SiCl_2$*	−2.18
SiH_2Cl_2	hole	$SiHCl_2$* + H*	−1.86
$SiHCl_3$	hole	$SiHCl$* + 2Cl*	−2.63
HCl	top1	H* + Cl*	−2.60
H_2	bridge	2H*	−1.96

[a]Here, * denotes a surface site.

Figure 3. (a) Total charge densities (TCD) and (b) charge density differences (CDD) of $SiCl_4$ adsorbed on the Si(100) surface. The green represents charge, and the blue (yellow) areas are electron aggregation (depletion). The isosurface values of TCD and CDD are 0.2 and ±0.02 e/Å^3, respectively.
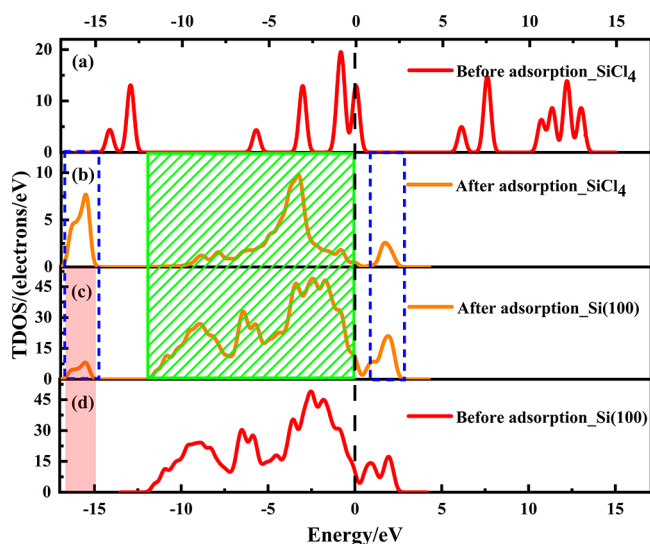
between the p orbital of the Cl1 atom and s, p orbitals of the Si1 atom in the energy range of −7.5 to 0 eV (the violet slash

Figure 4. Total density of states (TDOS) of $SiCl_4$ before adsorption (a) and after adsorption (b), Si(100) surface before adsorption (c) and after adsorption (d). The vertical black dashed line represents the Fermi level.
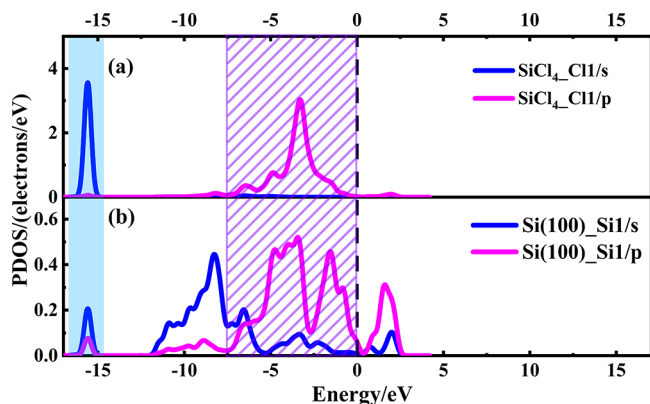

Figure 5. PDOS for (a) Cl1 atoms of $SiCl_4$ and (b) Si1 atoms of the Si(100) surface after adsorption. The vertical black dashed line represents the Fermi level.

box area), which also indicates that there are strong hybridizations among these atomic orbitals.

For $SiCl_2$, two different adsorption styles are considered. The first one is the $SiCl_2$ molecule adsorbed on the top2 site of the Si(100) surface vertically. There is an obvious charge overlap between the $SiCl_2$ molecules and Si(100) (Figure 6a), namely, the $SiCl_2$ molecule interacts strongly with Si(100). From the CDD (Figure 6b), we can find that significant charge accumulation occurs around the $SiCl_2$ molecule, indicating that extremely strong covalent bonds are formed on the surface; thus, $SiCl_2$ acts as an electron acceptor. The results of PDOS (Figure 6d) show that there exist three resonance peaks at about −8.76, −1.70, and 1.24 eV (the shaded blue part) between Si atoms of the $SiCl_2$ molecule and Si1 atoms of the Si(100) surface, which suggests that the strong interaction of Si−Si1 takes place. The other one is the $SiCl_2$ molecule adsorbed on the Si(100) surface in a parallel manner (Figure 6c), and its E_{ads} is calculated to be −1.80 eV. It should be noted that the $SiCl_2$ molecule undergoes dissociative chemisorption, and the Si−Cl bonds of the $SiCl_2$ molecule are stretched from 2.109 to 2.292 and 2.507 Å, respectively.
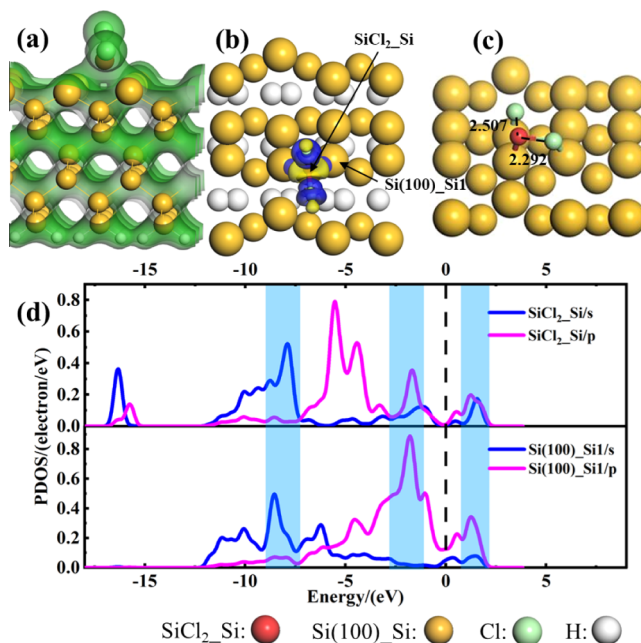

Figure 6. (a) TCD and (b) CDD of $SiCl_2$ adsorbed on the Si(100) surface in a vertical adsorption style, (c) $SiCl_2$ adsorbed on the Si(100) surface in a parallel adsorption style, (d) PDOS of Si atoms of $SiCl_2$ and Si1 atoms of the Si(100) surface. The blue (yellow) areas in panel (b) represent electron aggregation (depletion). The vertical black dashed line represents the Fermi level. The unit of bond length is Å. The isosurface values of TCD and CDD are 0.2 and ±0.02 e/Å³, respectively.

Nevertheless, from the view of adsorption energy, the vertical adsorption style of $SiCl_2$ is much more stable.

When SiH_2Cl_2 is adsorbed on the Si(100) surface, the charge of SiH_2Cl_2 overlaps with the charge of Si(100) (Figure 7a), indicating that the SiH_2Cl_2 molecule interacts with the Si(100) surface. The CDD (Figure 7b) shows that the electron accumulation is mainly localized on the SiH_2Cl_2 molecule, manifesting the electron-withdrawing property of SiH_2Cl_2. As displayed in Figure 7c, the H2-s orbital is greatly hybrid with Si4-s,p orbitals ranging from −9.50 to 0 eV (the violet slash box area), which indicates that the interactions between SiH_2Cl_2 and the Si(100) surface are strong.

In Figure 8a, there are charge exchanges and overlaps between $SiHCl_3$ and the Si(100) surface, indicating that the $SiHCl_3$ molecule strongly interacts with the Si(100) surface. The electron density around the adsorbed $SiHCl_3$ is significantly increased, as proved by the CDD in Figure 8b, and this suggests that many electrons of Si(100) are transferred to $SiHCl_3$. Additionally, the strong charge transfer indicates the bonding effect. The results of PDOS (Figure 8d) show that there exist two strong resonance peaks (the blue shaded part) at −15.60 eV between Cl3-s and Si4-s orbitals and at −3.28 eV between Cl3-p and Si4-s,p orbitals, respectively, resulting in the strong interaction between $SiHCl_3$ and the Si(100) surface.

Based on the above results, both SiH_2Cl_2 and $SiHCl_3$ are strongly adsorbed on the Si(100) surface at the hole site, and the adsorption strength of $SiHCl_3$ is larger than that of SiH_2Cl_2. Moreover, SiH_2Cl_2 is chemically dissociated into the H atom and $SiHCl_2$ molecule. The $SiHCl_3$ molecule can dissociate into the $SiHCl_2$ molecule and Cl atom after adsorption (Figure 8c). The corresponding adsorption energy is calculated to be −1.82 eV. When $SiHCl_3$ is adsorbed at the
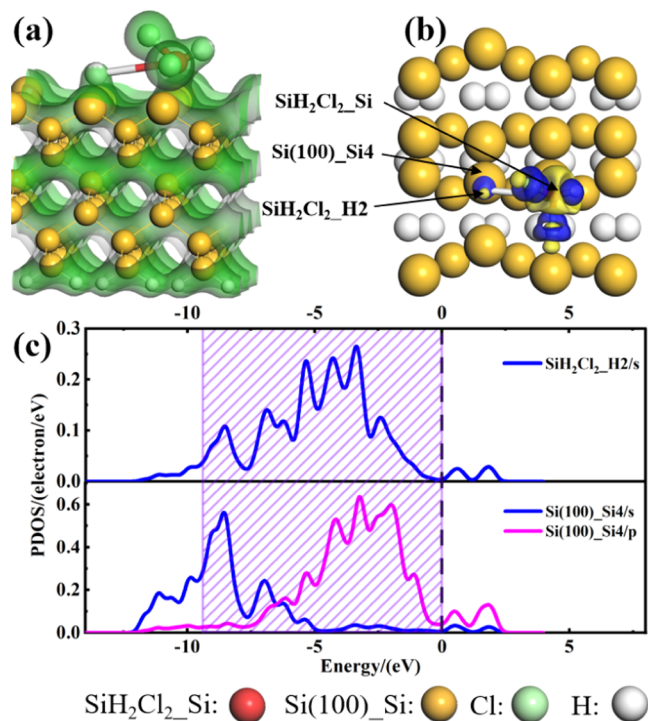
Figure 7. (a) TCD and (b) CDD of SiH_2Cl_2 adsorbed on the Si(100) surface, (c) PDOS of H2 atoms of SiH_2Cl_2 and Si4 atoms of the Si(100) surface. The green areas in panel (a) represent the charge density, and the blue (yellow) areas in panel (b) represent electron aggregation (depletion). The vertical black dashed line represents the Fermi level. The isosurface values of TCD and CDD are 0.2 and ±0.02 e/Å^3, respectively.
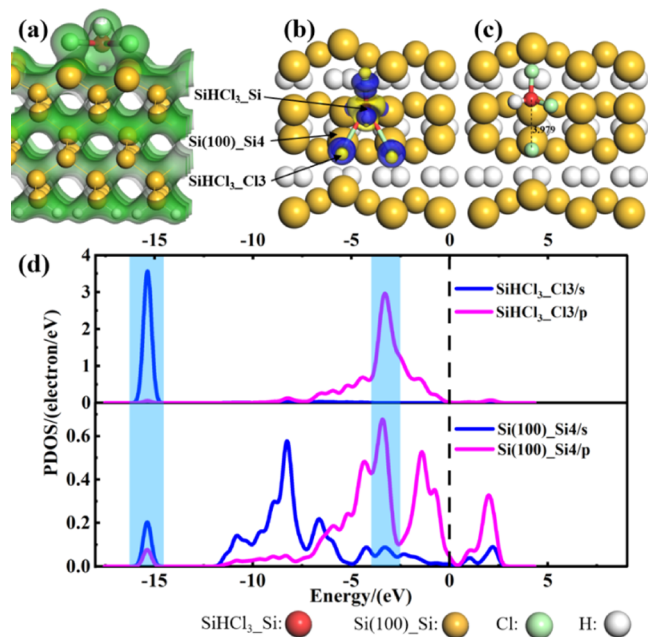

Figure 8. (a) TCD and (b) CDD of $SiHCl_3$ adsorbed on the Si(100) surface, (c) top view of the optimized $SiHCl_3$–Si(100) structure at the bridge site, (d) PDOS of Cl_3 atoms of $SiHCl_3$ and Si_4 atoms of the Si(100) surface. The green areas in panel (a) represent the charge density, the blue (yellow) areas in panel (b) represent electron aggregation (depletion). The vertical black dashed line represents the Fermi level. The unit of bond length is Å. The isosurface values of TCD and CDD are 0.2 and ±0.02 e/Å^3, respectively.

bridge site, one of the Si−Cl bonds in the $SiHCl_3$ molecule is stretched from 2.052 to 3.979 Å. It is worth noting that the calculated adsorption behavior of a single H atom and Cl atom on the hole site of the Si(100) surface is shown in Figure 9. These two atoms are bonding with the Si(100) surface, and the corresponding adsorption energies are calculated to be −3.82 and −4.21 eV, respectively. The Si(100) surface has a larger affinity with $SiHCl_3$ in comparison with SiH_2Cl_2, and this difference may be due to the fact that the adsorption capacity of a single Cl atom is stronger than that of the H atom on the Si(100) surface.

3.3. Adsorption of HCl and H_2 Molecules on the Si(100) Surface. From the TCD in Figure 10a, one can see that the charge overlaps between HCl and the Si (100) surface, which means that strong covalent bonds are formed between HCl and the Si(100) surface. Hou et al.[46] found that HCl was dissociative adsorbed on the Si(100) surface and H and Cl atoms adhered to the Si(100) surface, which is consistent with our conclusions in this work. From the CDD (Figure 10b), the HCl molecule is electron-rich, which indicates that the loss charges of the Si(100) surface are transferred to the HCl molecule. The results of PDOS (Figure 10c) show that the hybridizations between the Cl-s and Si4-s,p orbitals are found from −9.50 to −3.70 eV (the violet slash box area) in the valance band, and one strong resonance peak can also be observed at −3 eV (the blue shaded part), which indicates that the covalent bonding is formed between HCl and the Si(100) surface.

From the TCD in Figure 11a, the charge of the H_2 molecule overlaps that of the Si(100) surface when H_2 is adsorbed on the Si(100) surface, which indicates that there is an interaction between the H_2 molecule and the Si(100) surface. From the CDD (Figure 11b), one can see that the H_2 molecule adheres to the Si(100) surface after adsorption, which agrees well with the experimental observation by Dürr.[47] Additionally, the results of charge transfer indicate that the H_2 molecule acts as an electron acceptor, while the Si(100) surface acts as an electron donor. As shown in Figure 11c, the orbital hybridizations between the H_2 molecule and Si(100) surface mainly occur in the range of −9.50 to −1.25 eV (the violet slash box area), meaning that the H_2 molecule interacts strongly with the Si(100) surface.

Both the HCl and H_2 molecules undergo dissociative chemisorption. For HCl, the most stable adsorption site is the top1 site and the E_{ads} is −2.60 eV; both H and Cl atoms form stable chemical bonds with the Si(100) surface. For H_2, the most stable adsorption site is the bridge site and the E_{ads} is −1.96 eV; H atoms form stable chemical bonds with the Si(100) surface. Moreover, the H_2 adsorbed on other sites (top and hole sites) belongs to physical adsorption; thus, the adsorption of H_2 is more inclined to adsorb on the bridge site instead of the top and hole sites. These results suggest that Si(100) has a stronger adsorption ability for HCl in comparison with H_2. This difference could be due to the smaller radius of the H atom in comparison to the Cl atom, leading to the weaker interaction with surrounding Si surface atoms. Furthermore, the sticking coefficient of H_2 on silicon surfaces is extremely small.[48]

3.4. $SiCl_2$ Formation and $SiHCl_3$ Formation Mechanism. It is known that $SiCl_2$ is an essential intermediate product for the production of polysilicon by the Siemens process,[46] which can promote the formation of $SiHCl_3$.[49] Yadav[33] studied that the formation of $SiCl_2$ may arise from the
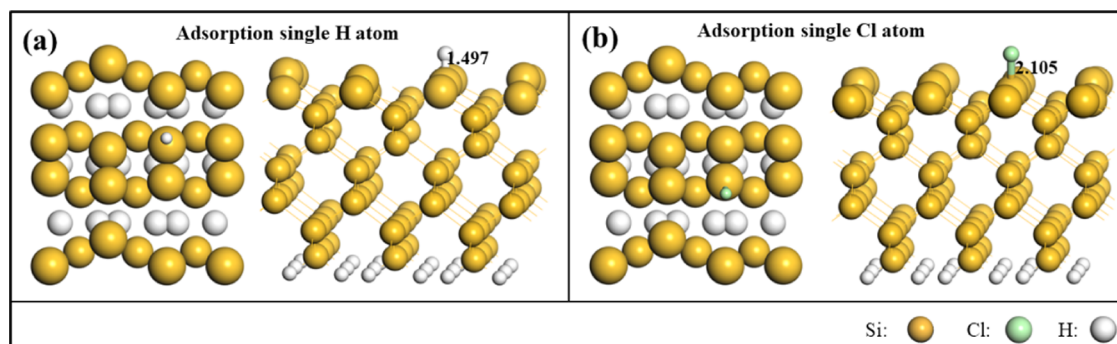
Figure 9. Lowest-energy structures of (a) single H atom and (b) single Cl atom absorbed on the Si(100) surface. The unit of bond length is Å.
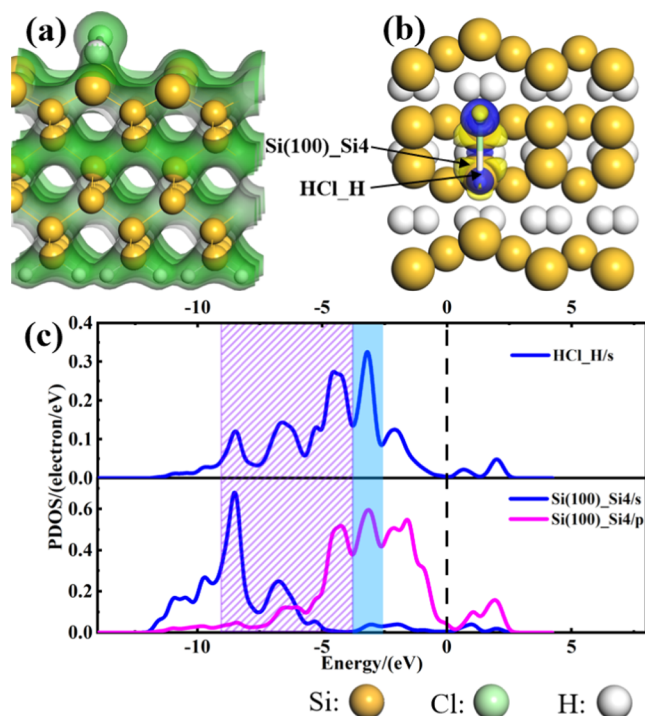

Figure 10. (a) TCD and (b) CDD of HCl adsorbed on the Si(100) surface, (c) PDOS of H atoms of HCl and Si4 atoms of the Si(100) surface. The green areas in panel (a) represent the charge density, the blue (yellow) areas in panel (b) represent electron aggregation (depletion). The vertical black dashed line represents the Fermi level. The isosurface values of TCD and CDD are 0.2 and ±0.02 e/Å³, respectively.

Figure 11. (a) TCD and (b) CDD of H_2 adsorbed on the Si(100) surface, (c) PDOS of H2 atoms of H_2 and Si4 atoms of the Si(100) surface. The green areas in panel (a) represent the charge density, the blue (yellow) areas in panel (b) represent electron aggregation (depletion). The vertical black dashed line represents the Fermi level. The isosurface values of TCD and CDD are 0.2 and ±0.02 e/Å³, respectively.

Si atoms of Si(100) and Cl atoms. There are three ways to form $SiCl_2$, that is, the $SiCl_4$/SiH_2Cl_2/$SiHCl_3$ molecule dissociates into $SiCl_2$. Our results show that $SiCl_4$, SiH_2Cl_2, and $SiHCl_3$ undergo dissociative chemisorption after they are adsorbed on the Si(100) surface. Moreover, the $SiCl_4$ adsorption leads to the formation of $SiCl_2$ (Figure 12a), which indicates that the $SiCl_2$ molecule is spontaneously formed during $SiCl_4$ adsorption. Specifically, the minimum energy path (MEP) to search for the involved transition state in $SiCl_2$ formation was obtained by LST/QST tools[34,50] in DMol³ code 8.0. The barrier energy E_a reported herein was calculated as follows

$$E_a = E_{TS} - E_{IS} \tag{5}$$

where E_{IS} and E_{TS} represent the total energy of the initial state (IS) and transition state (TS), respectively.
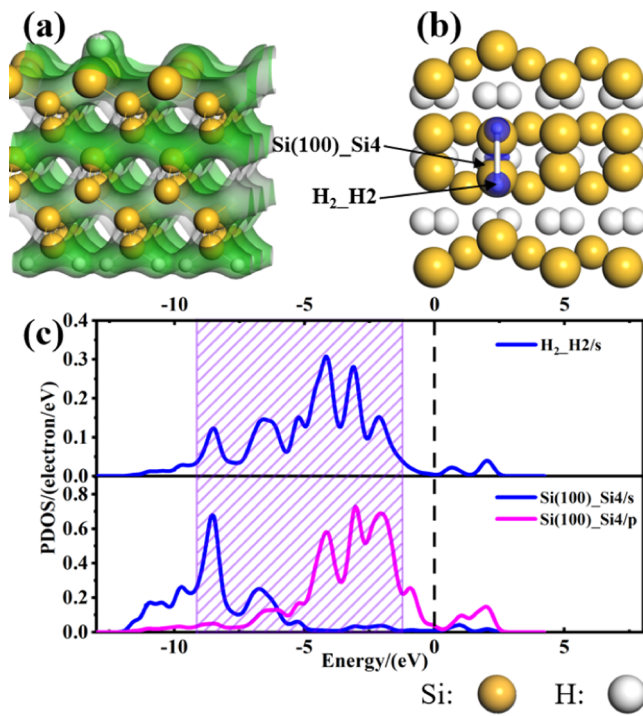
For SiH_2Cl_2 and $SiHCl_3$, they are only spontaneously dissociated into $SiHCl_2$ after adsorptions on the Si(100) surface, as illustrated in Figure 12b,c, whereas $SiHCl_2$ is hardly further dissociated on the Si(100) surface. Therefore, the transition of $SiHCl_2$ to $SiCl_2$ should overcome a certain energy barrier. As shown in Figure 13, the reaction of $SiHCl_2$ to $SiCl_2$ on Si(100) is exothermic with an energy of 44.38 kJ/mol, and the calculated reaction barrier is about 110.00 kJ/mol, which is smaller than that of $SiHCl_2$ dissociating into $SiCl_2$ on the Si(111) surface (147.90 kJ/mol).[34] In conclusion, $SiCl_4$ can be directly dissociated into $SiCl_2$ on the Si(100) surface. By contrast, SiH_2Cl_2 and $SiHCl_3$ molecules first dissociate into $SiHCl_2$* without zero energy barrier, and then, the $SiHCl_2$ molecule converted into $SiCl_2$ needs to overcome an energy barrier of 110.00 kJ/mol. Thus, $SiCl_4$ is more beneficial to
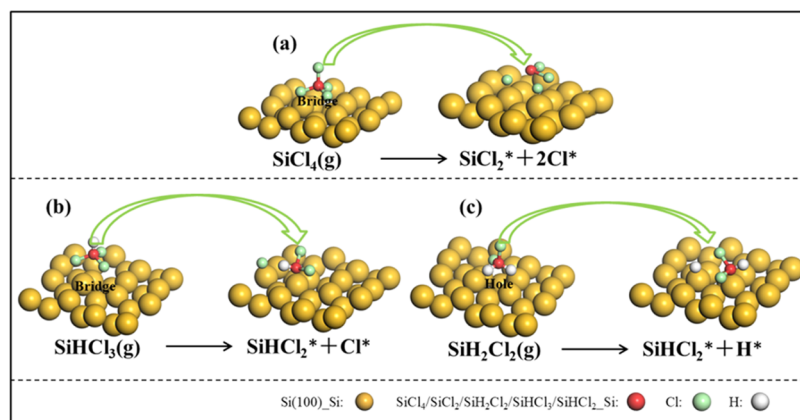
Figure 12. Pathway for the (a) SiCl$_4$ molecule dissociates into SiCl$_2$* + 2Cl*, (b) SiHCl$_3$ molecule dissociates into SiHCl$_2$ + Cl, and (c) SiH$_2$Cl$_2$ molecule dissociates into SiHCl$_2$ + H.
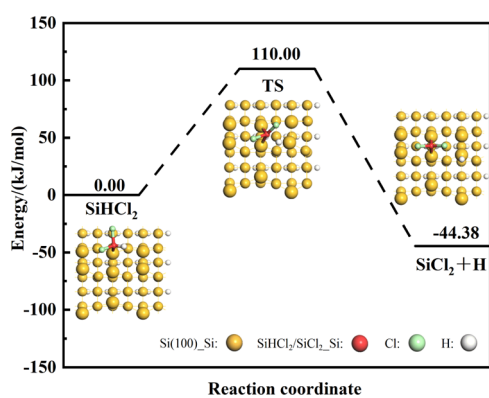
Figure 13. Potential energy profiles of SiHCl$_2$ dissociation into SiCl$_2$ + H.

compared with the other molecules. Hirshfeld charge analysis reveals that all of the adsorbed molecules on the Si(100) surface behave as electron acceptors. Moreover, strong interactions can be found between gas molecules and the Si(100) surface as proved by the analysis of TCD, CDD, and DOS. Additionally, SiCl$_2$ can be formed by SiCl$_4$ with zero barrier paths. However, SiH$_2$Cl$_2$ and SiHCl$_3$ can be spontaneously dissociated into SiHCl$_2$*, and then, the intermediate product SiHCl$_2$* needs to overcome an energy barrier of 110 kJ/mol to produce SiCl$_2$. Our results can provide a necessary theoretical basis for the reaction mechanism and experimental work of silicon tetrachloride hydrochlorination.

promote the formation of SiCl$_2$ compared with SiHCl$_3$ and SiH$_2$Cl$_2$ molecules.

The primary purpose of the hydrochlorination process is to convert SiCl$_4$ to SiHCl$_3$. However, it is difficult to convert all SiCl$_4$ to SiHCl$_3$ directly. SiCl$_2$ is a major intermediate in the hydrochlorination process, which is favorable to the formation of SiHCl$_3$.[48] Hence, SiCl$_2$ is a prime candidate and can react with the surface-adsorbed Cl and H atoms to produce SiHCl$_3$. The H and Cl required for SiCl$_2$ and SiHCl$_3$ would be supplied from HCl dissociative adsorption. Therefore, a possible reaction mechanism is proposed through the following basic processes

$$SiCl_4(g) \rightarrow SiCl_2^* + 2Cl^* \tag{6}$$

$$HCl(g) \rightarrow Cl^* + H^* \tag{7}$$

$$SiCl_2^* + H^* + Cl^* \rightarrow SiHCl_3(g) \tag{8}$$
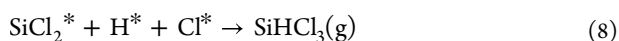
4. CONCLUSIONS

First-principles calculations were employed to investigate the adsorption behaviors of silicon tetrachloride (SiCl$_4$), silicon dichloride (SiCl$_2$), dichlorosilane (SiH$_2$Cl$_2$), trichlorosilane (SiHCl$_3$), HCl, and H$_2$ molecules on the Si(100) surface, and the electronic properties of different adsorption systems were analyzed. The results show that all of the gas molecules can bond with the Si(100) surface and even undergo dissociative chemisorption, and SiHCl$_3$ has stronger adsorption strength

■ AUTHOR INFORMATION

Corresponding Author

Zhifeng Nie − *Yunnan Key Laboratory of Metal-Organic Molecular Materials and Device, School of Chemistry and Chemical Engineering, Kunming University, Kunming 650214, China;* ● orcid.org/0000-0002-4342-9902; Email: niezf123@163.com

Authors

Yajun Wang − *Yunnan Key Laboratory of Metal-Organic Molecular Materials and Device, School of Chemistry and Chemical Engineering, Kunming University, Kunming 650214, China; School of Physical Science and Technology, Kunming University, Kunming 650214, China*

Qijun Guo − *Yunnan Key Laboratory of Metal-Organic Molecular Materials and Device, School of Chemistry and Chemical Engineering, Kunming University, Kunming 650214, China;* ● orcid.org/0000-0003-3915-6195

Yumin Song − *Yunnan Key Laboratory of Metal-Organic Molecular Materials and Device, School of Chemistry and Chemical Engineering, Kunming University, Kunming 650214, China*

Li Liu − *School of Metallurgy and Energy Engineering, Kunming University of Science and Technology, Kunming 650093, China; Kunming Engineering & Research Institute of Nonferrous Metallurgy Co., Ltd., Kunming 650051, China*

Complete contact information is available at:
https://pubs.acs.org/10.1021/acsomega.2c04502

Notes

■ REFERENCES

(1) Zou, X.; Ji, L.; Ge, J.; Sadoway, D. R.; Edward, T. Y.; Bard, A. J. Electrodeposition of crystalline silicon films from silicon dioxide for low-cost photovoltaic applications. *Nat. Commun.* **2019**, *10*, No. 5772.

(2) Villicaña-García, E.; Ramírez-Márquez, C.; Segovia-Hernández, J. G.; Ponce-Ortega, J. M. Planning of intensified production of solar grade silicon to yield solar panels involving behavior of population. *Chem. Eng. Process.: Process Intensif.* **2021**, *161*, No. 108241.

(3) Nie, Z.; Wang, Y.; Wang, C.; Guo, Q.; Hou, Y.; Ramachandran, P. A.; Xie, G. Mathematical model and energy efficiency analysis of Siemens reactor with a quartz ceramic lining. *Appl. Therm. Eng.* **2021**, *199*, No. 117522.

(4) Wan, Y.; Yan, D.; Xiao, J.; Chu, D.; Zhang, Y. Discussion on hydrogen quality detection methods for polysilicon production. *J. Phys.: Conf. Ser.* **2019**, *1347*, No. 012106.

(5) Braga, A.; Moreira, S.; Zampieri, P.; Bacchin, J.; Mei, P. New processes for the production of solar-grade polycrystalline silicon: A review. *Sol. Energy Mater. Sol. Cells* **2008**, *92*, 418−424.

(6) Liu, N.; Liu, X.; Wang, F.; Xin, F.; Sun, M.; Zhai, Y.; Zhang, X. CFD simulation study of the effect of baffles on the fluidized bed for hydrogenation of silicon tetrachloride. *Chin. J. Chem. Eng.* **2022**, *45*, 219−228.

(7) Ramírez-Márquez, C.; Contreras-Zarazúa, G.; Martín, M.; Segovia-Hernández, J. G. Safety, economic, and environmental optimization applied to three processes for the production of solar-grade silicon. *ACS Sustainable Chem. Eng.* **2019**, *7*, 5355−5366.

(8) Ding, W.-J.; Wang, Z.; Yan, J.; Xiao, W. CuCl-catalyzed hydrogenation of silicon tetrachloride in the presence of silicon: mechanism and kinetic modeling. *Ind. Eng. Chem. Res.* **2014**, *53*, 16725−16735.

(9) Kunioshi, N.; Moriyama, Y.; Fuwa, A. Kinetics of the conversion of silicon tetrachloride into trichlorosilane obtained through the temperature control along a plug-flow reactor. *Int. J. Chem. Kinet.* **2016**, *48*, 45−57.

(10) Yadav, S.; Chattopadhyay, K.; Singh, C. V. Solar grade silicon production: A review of kinetic, thermodynamic and fluid dynamics based continuum scale modeling. *Renewable Sustainable Energy Rev.* **2017**, *78*, 1288−1314.

(11) Wu, J.; Chen, Z.; Ma, W.; Dai, Y. Thermodynamic estimation of silicon tetrachloride to trichlorosilane by a low temperature hydrogenation technique. *Silicon* **2017**, *9*, 69−75.

(12) Lee, J. Y.; Lee, W. H.; Park, Y.-K.; Kim, H. Y.; Kang, N. Y.; Yoon, K. B.; Choi, W. C.; Yang, O.-B. Catalytic conversion of silicon tetrachloride to trichlorosilane for a poly-Si process. *Sol. Energy Mater. Sol. Cells* **2012**, *105*, 142−147.

(13) Wang, C.; Wang, T.; Li, P.; Wang, Z. Recycling of SiCl$_4$ in the manufacture of granular polysilicon in a fluidized bed reactor. *Chem. Eng. J.* **2013**, *220*, 81−88.

(14) Vorotyntsev, A. V.; Petukhov, A. N.; Vorotyntsev, I. V.; Sazanova, T. S.; Trubyanov, M. M.; Kopersak, I. Y.; Razov, E. N.; Vorotyntsev, V. M. Low-temperature catalytic hydrogenation of silicon and germanium tetrachlorides on the modified nickel chloride. *Appl. Catal., B* **2016**, *198*, 334−346.

(15) Ding, W.-J.; Yan, J.; Xiao, W. Hydrogenation of silicon tetrachloride in the presence of silicon: thermodynamic and experimental investigation. *Ind. Eng. Chem. Res.* **2014**, *53*, 10943−10953.

(16) Buehler, E. J.; Boland, J. J. Dimer preparation that mimics the transition state for the adsorption of H$_2$ on the Si (100)-2 × 1 surface. *Science* **2000**, *290*, 506−509.

(17) Kuzmin, M.; Lehtiö, J.-P.; Rad, Z.; Mäkelä, J.; Lahti, A.; Punkkinen, M.; Laukkanen, P.; Kokko, K. Dimer-vacancy defects on Si (100): The role of nickel impurity. *Appl. Surf. Sci.* **2020**, *506*, No. 144647.

(18) Hall, M. A.; Mui, C.; Musgrave, C. B. DFT Study of the adsorption of chlorosilanes on the Si (100)-2 × 1 Surface. *J. Phys. Chem. B* **2001**, *105*, 12068−12075.

(19) Ng, R. Q. M.; Tok, E.; Kang, H. C. Molecular mechanisms for disilane chemisorption on Si (100)-(2 × 1). *J. Chem. Phys.* **2009**, *130*, No. 114702.

(20) Pavlova, T. V.; Skorokhodov, E. S.; Zhidomirov, G. M.; Eltsov, K. N. Ab initio study of the early stage of Si epitaxy on the chlorinated Si(100) surface. *J. Phys. Chem. C* **2019**, *123*, 19806−19811.

(21) Andryushechkin, B. V.; Eltsov, K.; Kuzmichev, A.; Shevlyuga, V. Electron-induced interaction of condensed chlorine with Si (100). *Phys. Wave Phenom.* **2010**, *18*, 303−312.

(22) Anzai, K.; Kunioshi, N.; Fuwa, A. Analysis of the dynamics of reactions of SiCl$_2$ at Si (100) surfaces. *Appl. Surf. Sci.* **2017**, *392*, 410−417.

(23) Delley, B. Time dependent density functional theory with DMol^3. *J. Phys.: Condens. Matter* **2010**, *22*, No. 384208.

(24) Delley, B. From molecules to solids with the DMol^3 approach. *J. Chem. Phys.* **2000**, *113*, 7756−7764.

(25) Chen, L.; Cheng, Dg.; Chen, F.; Zhan, X. A density functional theory study on the conversion of polycyclic aromatic hydrocarbons in hydrogen plasma. *Int. J. Hydrogen Energy* **2020**, *45*, 309−321.

(26) Li, K.; Li, N.; Yan, N.; Wang, T.; Zhang, Y.; Song, Q.; Li, H. Adsorption of small hydrocarbons on pristine, N-doped and vacancy graphene by DFT study. *Appl. Surf. Sci.* **2020**, *515*, No. 146028.

(27) Hammer, B.; Hansen, L. B.; Nørskov, J. K. Improved adsorption energetics within density-functional theory using revised Perdew-Burke-Ernzerh of functionals. *Phys. Rev. B* **1999**, *59*, 7413.

(28) Shao, X.; Li, L.; Huang, S.; Song, Z.; Wang, K. First-Principles Calculations of Magnetic Moment Modulation of 3d Transition Metal Atoms Encapsulated in C$_{60}$/C$_{70}$ Cages on Si (100) Surfaces: Implications for Spintronic Devices. *ACS Appl. Nano Mater.* **2021**, *4*, 12356−12364.

(29) Pavlova, T. V.; Shevlyuga, V. M.; Andryushechkin, B. V.; Eltsov, K. N. Dangling bonds on the Cl-and Br-terminated Si (100) surfaces. *Appl. Surf. Sci.* **2022**, *591*, No. 153080.

(30) Baek, S. B.; Kim, D. H.; Kim, Y. C. Adsorption and surface reaction of bis-diethylaminosilane as a Si precursor on an OH-terminated Si (001) surface. *Appl. Surf. Sci.* **2012**, *258*, 6341−6344.

(31) Orazi, V.; Bechthold, P.; Jasen, P. V.; Faccio, R.; Pronsato, M. E.; Gonzalez, E. A. DFT study of methanol adsorption on PtCo (111). *Appl. Surf. Sci.* **2017**, *420*, 383−389.

(32) Grimme, S. Semiempirical GGA-type density functional constructed with a long-range dispersion correction. *J. Comput. Chem.* **2006**, *27*, 1787−1799.

(33) Yadav, S.; Singh, C. V. Molecular adsorption and surface formation reactions of HCl, H$_2$ and chlorosilanes on Si (100)-c(4 × 2) with applications for high purity silicon production. *Appl. Surf. Sci.* **2019**, *475*, 124−134.

(34) Peng, M.; Shi, B.; Han, Y.; Li, W.; Zhang, J. Crystal facet dependence of SiHCl$_3$ reduction to Si mechanism on silicon rod. *Appl. Surf. Sci.* **2022**, *580*, No. 152366.

(35) Nie, Z.; Wang, C.; Xue, R.; Xie, G.; Xiong, H. Two-dimensional FePc and MnPc monolayers as promising materials for SF$_6$ decomposition gases detection: Insights from DFT calculations. *Appl. Surf. Sci.* **2023**, *608*, No. 155119.

(36) Tang, Q.; Shen, H.; Yao, H.; Jiang, Y.; Li, Y.; Zhang, L.; Ni, Z.; Wei, Q. Formation mechanism of inverted pyramid from sub-micro to

micro scale on C-Si surface by metal assisted chemical etching temperature. *Appl. Surf. Sci.* **2018**, *455*, 283−294.

(37) Hannah, D. C.; Yang, J.; Podsiadlo, P.; Chan, M. K.; et al. On the origin of photoluminescence in silicon nanocrystals: pressure-dependent structural and optical studies. *Nano Lett.* **2012**, *12*, 4200−4205.

(38) Lim, T. B.; McNab, I. R.; Polanyi, J. C.; Guo, H.; Ji, W. Multiple Pathways of Dissociative Attachment: CH_3Br on Si (100)-2×1. *J. Am. Chem. Soc.* **2011**, *133*, 11534−11539.

(39) Czekala, P. T.; Lin, H.; Hofer, W. A.; Gulans, A. Acetylene adsorption on silicon (100)-(4 × 2) revisited. *Surf. Sci.* **2011**, *605*, 1341−1346.

(40) Nachimuthu, S.; Chen, T. R.; Yeh, C. H.; Hong, L. S.; Jiang, J. C. Combined density functional theory and microkinetics study to predict optimum operating conditions of Si (100) surface carbonization by acetylene for high power devices. *J. Phys. Chem. Lett.* **2021**, *12*, 4558−4568.

(41) Pabianek, K.; Krukowski, P.; Polański, K.; Ciepielewski, P.; Baranowski, J. M.; Rogala, M.; Kozłowski, W.; Busiakiewicz, A. Interactions of Ti and its oxides with selected surfaces: Si (100), HOPG (0001) and graphene/4H-SiC (0001). *Surf. Coat. Technol.* **2020**, *397*, No. 126033.

(42) Yao, X.; Wang, J.; Wu, G.; Goh, S. S.; Zhu, H.; Yang, S. W. Theoretical study on the self-assembly of 1, 3, 5-triethynylbenzene on Si (100) 2 × 1 and in situ polymerization via reaction with CO to fabricate a single surface-grafted polymer. *J. Mater. Chem. C* **2017**, *5*, 3585−3591.

(43) Ishikawa, H.; Fujima, K.; Adachi, H.; Miyauchi, E.; Fujii, T. Calculation of electronic structure and photoabsorption spectra of monosilane molecules SiH_4, SiF_4, and $SiCl_4$. *J. Chem. Phys.* **1991**, *94*, 6740−6750.

(44) Cao, M.; Gao, A.; Liu, Y.; Zhou, Y.; Sun, Z.; Li, Y.; He, F.; Li, L.; Mo, L.; Liu, R.; et al. Theoretical study on electronic structural properties of catalytically reactive metalloporphyrin intermediates. *Catalysts* **2020**, *10*, 224.

(45) Brohi, R. O. Z.; Khuhawar, M. Y.; Mahar, R. B.; Ibrahim, M. A. Novel bimetallic nano particles for sorption of mercury (II) from drinking water: adsorption experiment and computational studies. *J. Water Process Eng.* **2021**, *39*, No. 101727.

(46) Hou, H.-Y.; Wu, H.; Chung, J.; Lin, D. Adsorption of diatomic interhalogens on the Si (100) and Ge (100) surfaces. *J. Phys. Chem. C* **2011**, *115*, 13262−13267.

(47) Dürr, M.; Hu, Z.; Biedermann, A.; Höfer, U.; Heinz, T. Real-space study of the pathway for dissociative adsorption of H_2 on Si(001). *Phys. Rev. Lett.* **2002**, *88*, No. 046104.

(48) Kunioshi, N.; Anzai, K.; Ushijima, H.; Fuwa, A. Effects of cluster size on calculation of activation energies of silicon surface reactions with H_2 and HCl. *J. Cryst. Growth* **2015**, *418*, 115−119.

(49) Yadav, S.; Singh, C. V. First principles investigation of HCl, H_2, and chlorosilane adsorption on Cu_3Si surfaces with applications for polysilicon production. *J. Phys. Chem. C* **2018**, *122*, 20252−20260.

(50) Wang, Z.; Zhao, J.; Cai, Q.; Li, F. Computational screening for high-activity MoS_2 monolayer-based catalysts for the oxygen reduction reaction via substitutional doping with transition metal. *J. Mater. Chem. A* **2017**, *5*, 9842−9851.